Vol. 26 • No. 23 • June 18 • 2014

D10488

www.advmat.de

ADVANCED MATERIALS

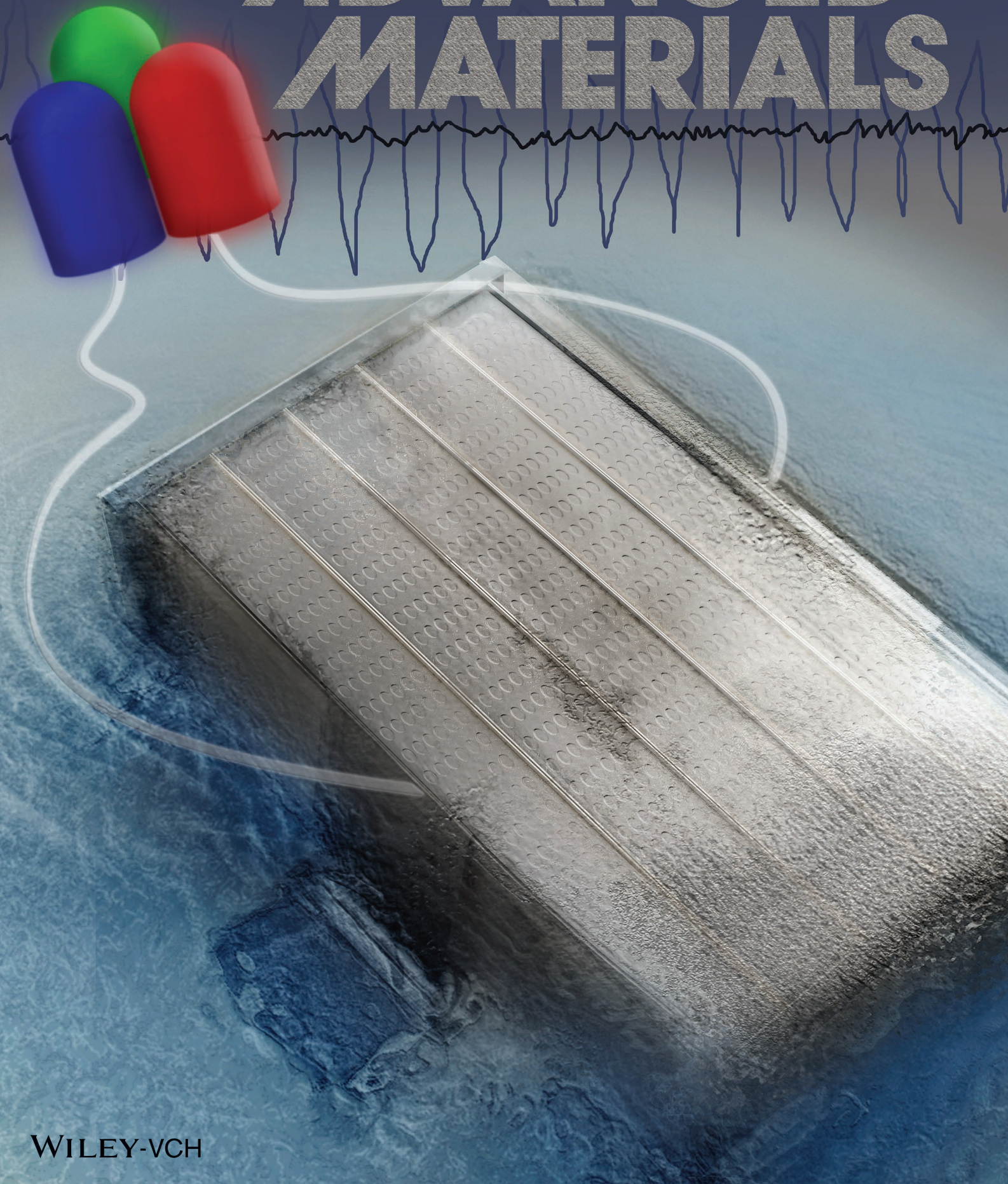

WILEY-VCH

Materials, Designs, and Operational Characteristics for Fully Biodegradable Primary Batteries

*Lan Yin, Xian Huang, Hangxun Xu, Yanfeng Zhang, Jasper Lam, Jianjun Cheng, and John A. Rogers**

Transient electronics is an emerging technology, the key attribute of which is an ability to physically disappear, entirely or in part, in a controlled manner after a period of stable operation.[1] Potential applications include zero-waste environmental sensors, hardware-secure memory modules, and temporary biomedical implants. For this third example, biodegradable electronics built using water-soluble, biocompatible active and passive materials provide multifunctional operation to assist or monitor a transient biological event, such as wound healing.[1–5] Biodegradable power supply is an essential component for many such systems. Demonstrated strategies range from degradable radio frequency power transfer modules,[6] silicon based photovoltaics[1] and mechanical energy harvesters.[7] Primary batteries represent versatile options that can complement these and other possibilities. One design involves adapted versions of water-activated battery technologies, in which the constituent materials are transient.[8,9] Kim et al. recently reported an edible sodium ion battery[8] with biologically derived melanin as an electrode.[10] Although few technical details are available, recent announcements suggest the use of isolated galvanic pairs of Mg and a copper salt as small-capacity power sources for ingestible pharmaceuticals that are activated upon exposure to the digestive tract;[11] the structures do not, however, exist as proper batteries, in the conventional sense, nor do they offer output powers useful for general classes of bioresorbable electronics. Magnesium (Mg) is, however, an appealing anode material due to its high energy density, long shelf-life and desirable biocompatibility.[12–14] Conventional Mg primary batteries use cathode materials (e.g., non-conductive AgCl, CuCl and MnO_2 for high performance, or copper, carbon and stainless steel for long lifetime)[13,15] that are either non-degradable, toxic, and/or environmentally hazardous. Such devices also involve long-lasting current collectors and packages.[13,16] Replacing the cathode materials with biodegradable metals[17–20] (e.g., iron (Fe), tungsten (W) or molybdenum (Mo)) together with biodegradable polymers (e.g., polyanhydrides)[21] for packaging creates an opportunity for the construction of fully transient batteries that can degrade, without harm, in biofluids or groundwater. In this design, the metallic cathode substitution reduces the operating voltages and current densities, but the overall performance can be compensated by monolithically integrating stacks of cells in series to increase the voltage and/or by enlarging the electrode area to increase the output current. Moreover, metal cathodes have the additional benefit that they simplify the assembly process. Here, the metal itself can serve as the current collector, thereby eliminating conductive binders that are required for standard materials such as AgCl or CuCl.

The water-activated primary batteries that we report here involve constituent materials that are all degradable, environmentally benign and biocompatible. Magnesium foils serve as the anodes, while metal foils based on Fe, W or Mo serve as the cathodes; the packages are formed with polyanhydrides[22–24] (see Figure S1, Supporting Information, for the synthetic scheme). Systematic studies reveal the achievable performance and the mechanisms for anode dissolution in single cells. Multi-cell packs that use Mg and Mo foils illustrate scalability in power, and include demonstrations in the powering of light-emitting diodes (LEDs) and radio transmitters.

The performance of single cell batteries that consist of Mg-X (X = Fe, W, or Mo) metal foils can be evaluated most conveniently by use of a PDMS liquid chamber filled with phosphate buffered saline (PBS) as the electrolyte. The testing structure appears in **Figure 1**a. The discharging behavior with an anode-cathode spacing of ≈2 mm is summarized in Figure 1b, for the case of a constant discharge current density (0.1 mA cm^{-2}). The operating voltages are ≈0.75 V, ≈0.65 V and ≈0.45 V for Fe, W and Mo, respectively. In each case, the voltage is stable for at least 24 hours. The lifetime is limited by the depletion of the active material (Mg). For similar levels of discharging current,

Prof. J. A. Rogers
Department of Materials Science and Engineering
Beckman Institute for Advanced Science and Technology
and Frederick Seitz Materials Research Laboratory
University of Illinois at Urbana-Champaign
Urbana, IL 61801, USA
E-mail: jrogers@illinois.edu

Dr. L. Yin, Dr. X. Huang
Department of Materials Science and Engineering
Beckman Institute for Advanced Science and Technology
and Frederick Seitz Materials Research Laboratory
University of Illinois at Urbana-Champaign
Urbana, IL 61801, USA

Prof. H. Xu
CAS Key Laboratory of Soft Matter Chemistry
Department of Polymer Science and Engineering
University of Science and Technology of China
Hefei, Anhui 230026, P. R. China

Dr. Y. Zhang, Prof. J. Cheng
Department of Materials Science and Engineering
University of Illinois at Urbana-Champaign
Urbana, IL 61801, USA

Mr. J. Lam
College of Liberal Arts and Sciences
University of Illinois at Urbana-Champaign
Urbana, IL 61801, USA

DOI: 10.1002/adma.201306304

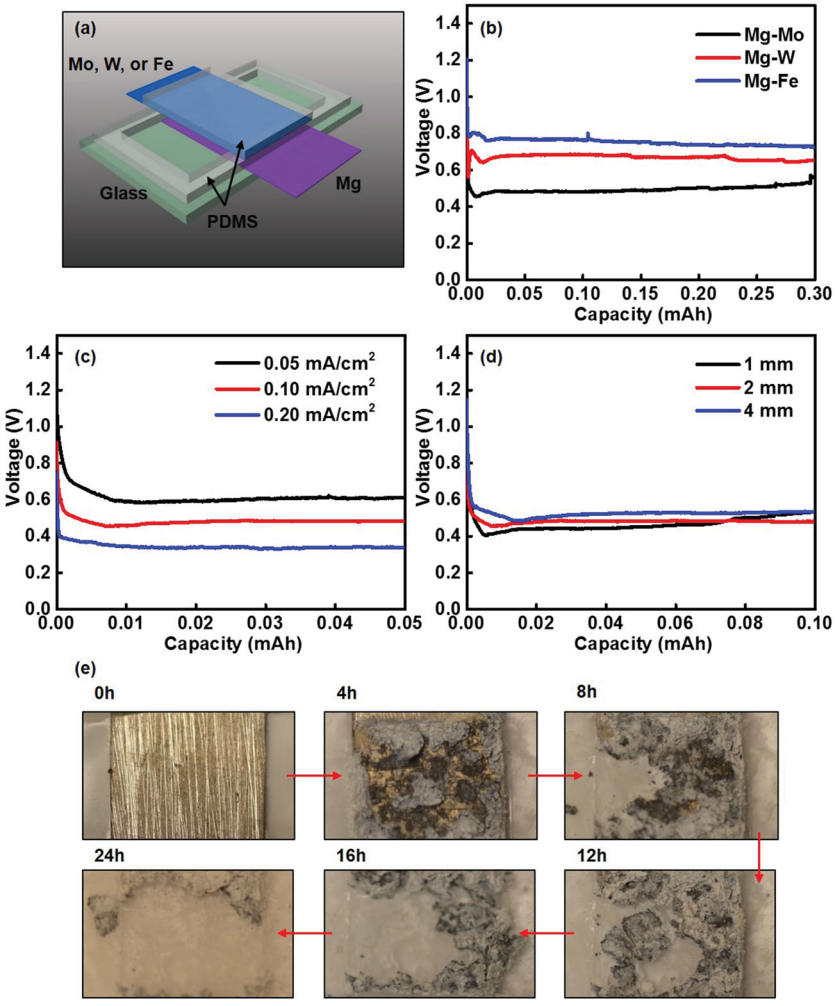

Figure 1. a) Configuration of a single cell Mg-X battery for performance evaluation; b) discharging behavior of a Mg-X battery under constant current (0.1 mA cm^{-2}); c) effects of discharging current density on Mg-Mo battery performance; d) effects of anode-cathode spacing on Mg-Mo battery performance; e) optical images of a Mg foil at various stages of degradation during discharging a Mg-Mo battery (0.1 mA cm^{-2}).

the observed output voltages are comparable to those in Mg deep seawater batteries with stainless steel cathodes,[15] but lower than conventional devices that use Mg/AgCl or Mg/CuCl (≈1.5–1.6 V).[13] Increasing the discharge current density lowers the output voltage, as shown in Figure 1c for Mg-Mo. Increasing the spacing between the anode and cathode from 1 mm to 4 mm does not obviously change the observed behaviors (Figure 1d). As illustrated in Figure 1e, during discharging (Mg-Mo battery, 0.1 mA cm^{-2}), Mg gradually degrades due to reactions associated with operation, as well as those due to corrosion (self-discharging). As can be seen from the Figure 1e, degradation of Mg is non-uniform (pitting type corrosion). White deposits, consistent with $Mg(OH)_2$, often appear on the surface of the foil.[25]

The main electrochemical reactions of the battery are as follows:[15,16]

i) Anode

$$Mg \rightarrow Mg^{2+} + 2e^{-} \quad (1)$$

The following side reaction takes place simultaneously:

$$Mg + 2H_2O \rightarrow Mg(OH)_2 + H_2 \quad (2)$$

ii) Cathode

$$O_2 + 2H_2O + 4e^{-} \rightarrow 4OH^{-}\,(\text{oxygen reduction}) \quad (3)$$

Or

$$2H_2O + 2e^{-} \rightarrow H_2 + 2OH^{-}\,(\text{hydrogen evolution}) \quad (4)$$

Oxygen reduction at the cathode site produces a higher potential compared to that for hydrogen reduction. The electrolyte typically contains a small amount of oxygen, such that the associated current densities are limited by diffusion of oxygen to the cathode surface. Hydrogen evolution enables improved current density, but with reduced output voltage.

To evaluate the possible reactions, potentials between Mg-Mo electrodes and potentials of individual electrodes vs. reference electrode (Ag/AgCl) as a function of discharge current density were investigated (scan rates: 0.01 mA cm^{-2} s^{-1}). As shown in **Figure 2**a, the Mg-Mo voltage exhibits a significant decrease at a current density up to 0.15 mA cm^{-2} and then switches to a slower decrease, which is mainly attributed to the characteristics of current dependence of the cathodic reaction (i.e. the Mo site). This reaction gives a potential –(0.6–0.7) V vs. Ag/AgCl reference electrode at a discharge current density of 0.1 mA cm^{-2}. This potential is less than the oxygen reduction potential (0.179 V vs. Ag/AgCl) and higher than the hydrogen evolution potential (–1.05 V vs. Ag/AgCl), suggesting that both types of reactions could take place. The cathodic reaction shifts completely to hydrogen evolution (–(1.2–1.3) V vs. Ag/AgCl) at a current density of 1 mA cm^{-2}, with a significant increase of the amount of visible hydrogen bubbles at the cathode. The significant decrease in voltage of Mg-Mo battery (Figure 2a) therefore mainly results from a change of the cathodic reaction from oxygen reduction to hydrogen evolution. Evaluations of electrochemical impedance were also conducted for the Mg-Mo electrodes (Figure 2b,c) as well as individual Mg and Mo electrodes at a discharge current density of 0.1 mA cm^{-2} (Figure 2d). These results suggest an electrolyte resistance of ≈30 Ω cm^{-2}, and an impedance of ≈3000 Ω cm^{-2} at low frequency, which mainly arises from the cathodic reaction (Figure 2d).

With 1 cm^2 active area, a with 50 μm thick Mg foil and an 8 μm thick Mo foil, this type of battery contains 8.7 mg Mg and 8.2 mg Mo, and offers a measured capacity of ≈2.4 mAh (0.1 mA cm^{-2} for 24 hours), corresponding to a specific capacity ≈276 mAh g^{-1} (normalized with anode mass). The amount of Mg is comparable

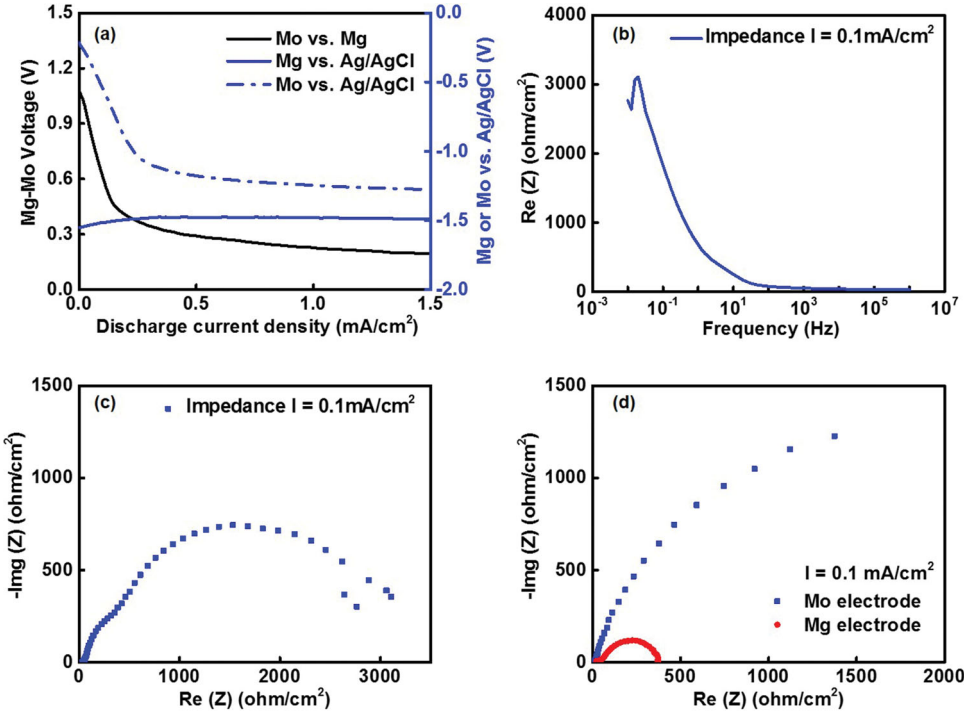

Figure 2. a) Voltage current density characteristics of a Mg-Mo battery and individual electrodes; b,c) electrochemical impedance between Mg-Mo electrodes (discharge current density of 0.1 mA cm^{-2}); d) electrochemical impedance of individual Mo and Mg electrodes respectively (discharge current density of 0.1 mA cm^{-2}).

to that in a single biodegradable Mg coronary arterial stent (≈3–6 mg).[19] Due to the corrosion of Mg foils during operation, together with impurities that might accelerate self-discharging, the measured capacity is lower than the theoretical capacity of Mg (2.2 Ah g^{-1}). Nevertheless, compared to the recently reported biodegradable melanin sodium-ion battery,[10] the Mg battery exhibits slightly higher stable voltage (≈0.4–0.7 V), higher discharge current density (0.1 mA cm^{-2}), longer lifetime (at least 24 hours) and higher specific capacity (≈276 mAh g^{-1}). The shelf time of a non-activated Mg battery can be long, due to a reasonable resistance to Mg oxidation in air.[14] If activated by PBS, the battery will lose roughly half of its capacity in 1–2 days, due to corrosion of the Mg foil.[26,27]

Stacking individual Mg cells in series increases the output voltage. A stacked configuration of four Mg-Mo cells appears in **Figure 3**a; the actual battery is in Figure 3b. Here, the dimension of each metal foil is 3 cm × 1.3 cm, corresponding to an area of 3.9 cm^2. The anode-cathode spacing for each Mg-Mo cell is ≈4 mm. The total weight of the stacked battery is ≈3.5 g, including 0.14 g Mg and 0.13 g Mo and the encasing materials. A thin layer of polyanhydride serves as a spacer (≈0.5 mm) to prevent electrical shorts between single cells, physically separating the electrolytes for each chamber. A Mo paste made of Mo powder and a water-soluble sodium carboxymethyl cellulose glue provides electrical connections between the individual cells, buried in the polyanhydride encasement to prevent shorts. Discharging the battery at a constant current density (0.1 mA cm^{-2}) gives a stable voltage output ≈1.5–1.6 V for up to 6 hours as shown in Figure 3c. The slow degradation in voltage that follows this period occurs at a time earlier than that of a single battery cell, possibly due to leakage between cells that can arise from pitting corrosion of the foils and/or water permeation through or degradation of the polyanhydride spacers. As shown in Figure 3d, a porous thin polyanhydride film (≈0.5 mm) can be used as a top cover to confine the electrolyte. Small pores (≈0.5 mm) in this film enable the release of hydrogen gas, but serve as a barrier to retain the electrolyte due to a positive contact angle (≈45°) of the polyanhydride (Figure S2, Supporting Information). Figure 3e demonstrates transience of the battery. The polyanhydride encasement degrades first to leave partially dissolved Mg and Mo foils after 11 days in PBS at 37° C. Accelerating the dissolution by increasing the temperature to 85 °C leads to elimination of the Mo foils after another 8 days.

As shown in **Figure 4**d, the stacked Mg-Mo battery can power a conventional LED (threshold voltage ≈1.6 V). A simple Colpitts oscillator circuit was designed to generate a radio frequency of 58 MHz and transmits the signal through an electrical small dipole antenna as shown in Figure 4a. To power such a circuit, a voltage of 1.5 V and a total current of ≈0.7 mA are required. The electrode area of the Mg-Mo stacked battery was therefore increased to 3 cm × 3.5 cm (10.5 cm^2), as shown in Figure 4c. The radio circuit powered by such battery successfully generates a signal approximately 30 MHz in frequency, which is lower than the designed frequency due to the frequency-dependent values of the passive components in the circuit. A signal analyzer connected by a hand-wound whip antenna can capture this signal ≈2 cm away at a level of –60 dBm as shown in Figure 4b. Longer transmission distance can be achieved by proper impedance matching both at the radio circuit and the signal analyzer.

The results presented here indicate a range of options in transient batteries, with dissolvable metals as the electrodes

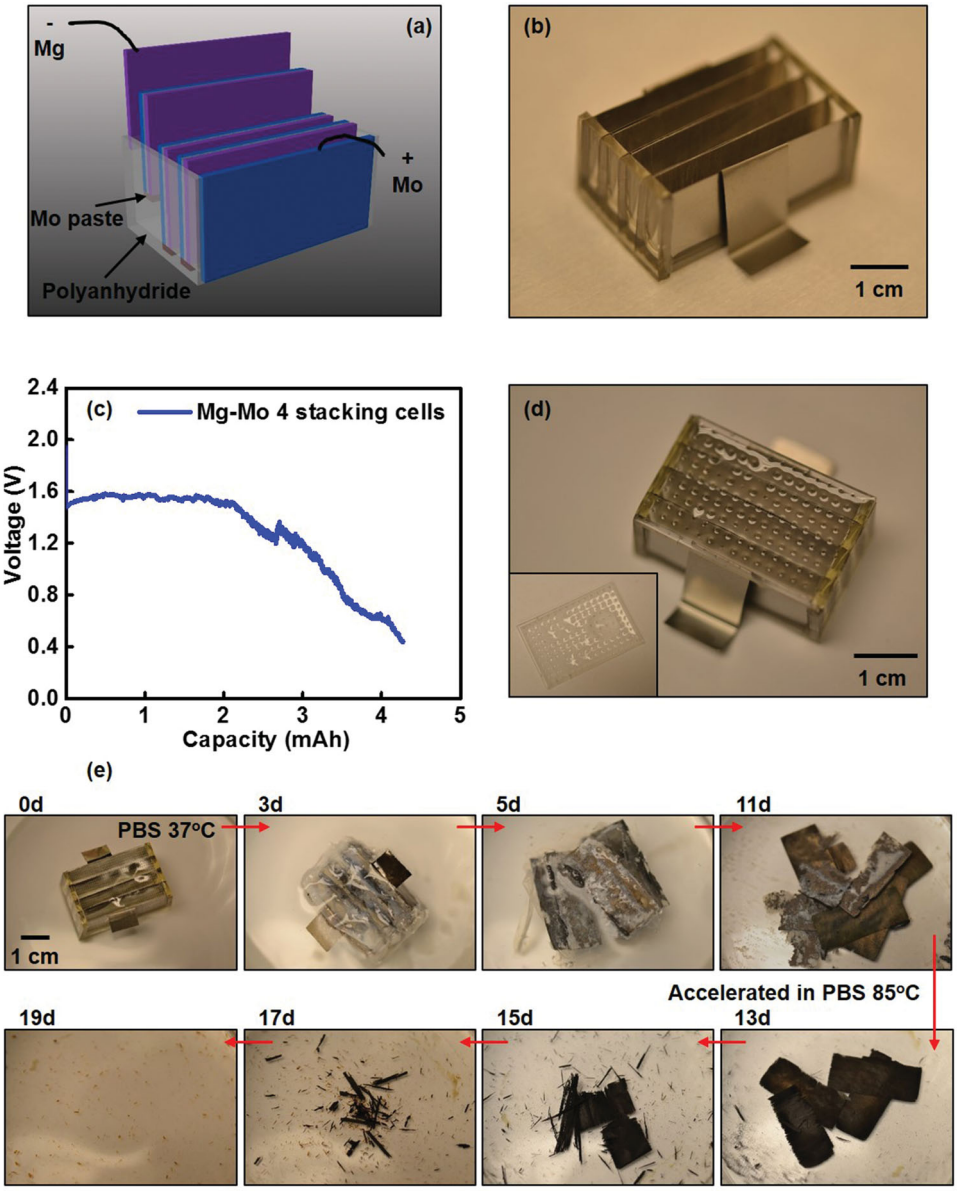

Figure 3. a) Configuration of a battery pack that consists of four Mg-Mo cells in series; b) optical images of the battery; c) discharging behavior (0.1 mA cm^{-2}); d) top porous polyanhydride cover to confine the electrolytes; e) dissolution of the battery.

and biodegradable polymers as barrier layers and encasements. Voltage and current levels that can be achieved enable operation of realistic devices of potential practical importance for biodegradable electronics. Opportunities for future developments include foils with thickness or/and surface treatment designed for controlling the transience times, schemes for programmable activation/deactivation of the battery to preserve the overall lifetime, and miniaturized cells for implantable sensors. Implantable batteries require power efficient designs, to allow operation with batteries at sizes compatible with use in the body. As with most battery technologies, size and total power capacity are tightly linked. The power supply requirements, therefore, are important to consider. For example, the average power consumption of published classes of low power wireless implantable sensing platforms (<0.5 V) can be <0.5 μW (averaged over standby and active periods).[28] In our transient batteries, Mg is the critical component and largely determines the capacity. The cathodic electrode serves simply as a reaction site, and can therefore be ultrathin. Based on data reported from our large devices (i.e. energy efficiency of ≈13%) the minimum size of a battery (i.e., the active component) needed to operate a wireless implantable sensing platform can be ≈5 mm × 5 mm, with a thickness of ≈1 μm, 30 μm, and 3460 μm for operation for 1 day, 1 month, or 1 year, respectively. Even if one assumes that the package, the cathode and the electrolyte double the overall dimensions, the sizes of these batteries are fully compatible with use in implants. In all such cases, the basic materials and architectures described here present simple and scalable batteries that provide biocompatible and environmentally benign sources of power.

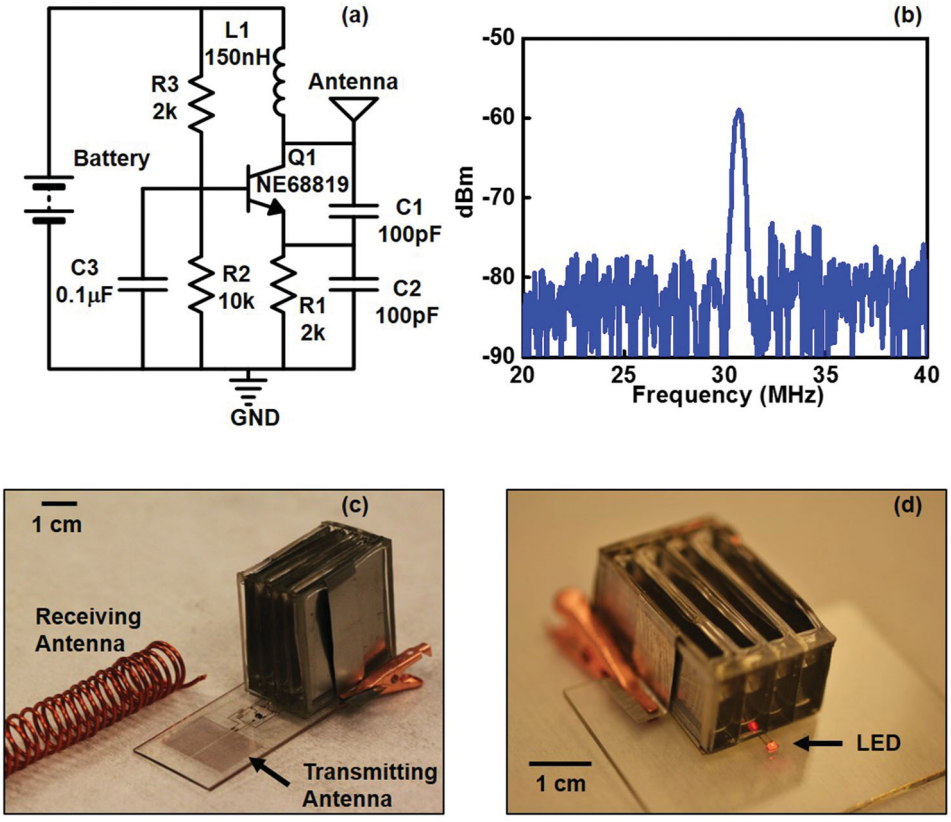

Figure 4. a) Radio circuit design; b) radio signal wirelessly received by a signal analyzer; c) battery powered operation of a radio circuit; d) battery powered operation of a red LED.

Experimental Section

Single cell batteries involved metal foils, selected from the following: Mg (50 μm thick), Fe (25 μm thick), W (25 μm thick), and Mo (25 μm thick). Mg foils were purchased from GalliumSource, LLC, Scotts Valley, CA, and Fe, W, and Mo foils were purchased from Goodfellow Corporation, Coraopolis, PA. The foils were cut into 1 cm × 2 cm strips. PDMS serves as the chamber materials and fix metal foils on glass. The backsides of the metal foils were also covered by PDMS to define the exposed area to be 1 cm^2. The anode-cathode spacing was controlled by a PDMS spacer. Stacks of such single cell batteries were fabricated by connecting four Mg-Mo cells. Foils were cut into 3 cm × 1.3 cm and a layer of polyanhydride spacer was laminated in between the cells. Polyanhydride was also used to encase metal foils and form the electrolyte chamber, by processes of casting with PDMS molds. UV-curable polyanhydride pre-cured polymer was prepared by mixing pentaerythritol tetrakis (3-mercaptopropionate), 4-pentenoic anhydride, and poly(ethylene glycol) diacrylate (molar ratio of 5:7:3) with the addition of 2,2-dimethoxy-2-phenylacetophenone (0.4 wt%) as the photoinitiator (all chemicals were purchased from Sigma-Aldrich Corporation, St. Louis, MO). The pre-cured polymer was molded using a PDMS mold and cured under UV-light (6 mW cm^{-2}) for 10 minutes. Mo paste was used to connect individual cells. These connections were buried in the polyanhydride encasement to prevent electrical shorts. The Mo paste was made by mixing Mo powder (10 μm) and sodium carboxymethyl cellulose with Mw ≈250 000 (Sigma-Aldrich Corporation, St. Louis, MO). The top polyanhydride cover with multiple pores (0.5 mm) was made by casting against a PDMS mold. In both single battery cells and multiple stacked cells, phosphate buffered saline served as the electrolyte and was injected into the chamber with a syringe. Dissolution of the stacked battery system was carried out in PBS (refreshed everyday) on a hot plate at 37 °C and later at 85 °C to accelerate the dissolution. Mo foil with a thickness 8 μm (Goodfellow Corporation, Coraopolis, PA) was used for the stacking battery to reduce the dissolution time.

Battery performance was measured by a Gamry potentialstat Reference 600 (Gamry Instruments, Warminster, PA) under a constant current discharging module using two-electrode configuration. Reactions and galvanostatic electrochemical impedance of electrodes were evaluated by a three-electrode configuration, with Ag/AgCl as the reference electrode (Bioanalytical Systems, Inc., West Lafayette, IN).

The radio and LED circuits were fabricated by patterning a bilayer of Cr/Au (5 nm/200 nm) on a glass substrate. Electronic components (Digi-Key Corporation, Thief River Falls, MN) were mounted on the Au pads by silver paste to build the functional circuits. The wireless signals were received by a CXA N9000A signal analyzer (Agilent Technologies, Santa Clara, CA).

Supporting Information

Supporting Information is available from the Wiley Online Library or from the author.

Acknowledgements

Financial support from DARPA and an NSF INSPIRE grant is acknowledged. Shimin Mao is acknowledged for contact angle measurements. This work was carried out in part in the Frederick Seitz Materials Research Laboratory Central Facilities, University of Illinois.

Received: December 28, 2013
Revised: February 5, 2014
Published online: March 20, 2014

[1] S.-W. Hwang, H. Tao, D.-H. Kim, H. Cheng, J.-K. Song, E. Rill, M. A. Brenckle, B. Panilaitis, S. M. Won, Y.-S. Kim, Y. M. Song, K. J. Yu, A. Ameen, R. Li, Y. Su, M. Yang, D. L. Kaplan, M. R. Zakin, M. J. Slepian, Y. Huang, F. G. Omenetto, J. A. Rogers, *Science* **2012**, *337*, 1640.
[2] C. J. Bettinger, Z. Bao, *Adv. Mater.* **2010**, *22*, 651.
[3] M. Irimia-Vladu, P. A. Troshin, M. Reisinger, L. Shmygleva, Y. Kanbur, G. Schwabegger, M. Bodea, R. Schwödiauer, A. Mumyatov, J. W. Fergus, V. F. Razumov, H. Sitter, N. S. Sariciftci, S. Bauer, *Adv. Funct. Mater.* **2010**, *20*, 4069.
[4] D. H. Kim, J. Viventi, J. J. Amsden, J. L. Xiao, L. Vigeland, Y. S. Kim, J. A. Blanco, B. Panilaitis, E. S. Frechette, D. Contreras, D. L. Kaplan, F. G. Omenetto, Y. G. Huang, K. C. Hwang, M. R. Zakin, B. Litt, J. A. Rogers, *Nat. Mater.* **2010**, *9*, 511.
[5] D. H. Kim, Y. S. Kim, J. Amsden, B. Panilaitis, D. L. Kaplan, F. G. Omenetto, M. R. Zakin, J. A. Rogers, *Appl. Phys. Lett.* **2009**, 95.
[6] S.-W. Hwang, X. Huang, J.-H. Seo, J.-K. Song, S. Kim, S. Hage-Ali, H.-J. Chung, H. Tao, F. G. Omenetto, Z. Ma, J. A. Rogers, *Adv. Mater.* **2013**, *25*, 3526.
[7] C. Dagdeviren, S.-W. Hwang, Y. Su, S. Kim, H. Cheng, O. Gur, R. Haney, F. G. Omenetto, Y. Huang, J. A. Rogers, *Small* **2013**, *9*, 3398.
[8] Y. J. Kim, S.-E. Chun, J. Whitacre, C. J. Bettinger, *J. Mater. Chem. B* **2013**, *1*, 3781.
[9] H. Jimbo, N. Miki, *Sens. Actuators, B* **2008**, *134*, 219.
[10] Y. J. Kim, W. Wu, S.-E. Chun, J. F. Whitacre, C. J. Bettinger, *Proc. Natl. Acad. Sci. USA* **2013**, *110*, 20912.
[11] Proteus Digital Health, http://www.proteus.com/ (accessed December 2013).
[12] S. Keim, J. G. Brunner, B. Fabry, S. Virtanen, *J. Biomed. Mater. Res., Part B* **2011**, *96B*, 84.
[13] T. B. Reddy, D. Linden, *Linden's Handbook of Batteries*, McGraw-Hill, New York **2011**.
[14] *Uhlig's Corrosion Handbook*, 3rd ed., (Ed. R. W. Revie), John Wiley & Sons, Hoboken, NJ **2011**.
[15] W. S. D. Wilcock, P. C. Kauffman, *J. Power Sources* **1997**, *66*, 71.
[16] K. Vuorilehto, *J. Appl. Electrochem.* **2003**, *33*, 15.
[17] L. Yin, H. Cheng, S. Mao, R. Haasch, Y. Liu, X. Xie, S.-W. Hwang, H. Jain, S.-K. Kang, Y. Su, R. Li, Y. Huang, J. A. Rogers, *Adv. Funct. Mater.* **2014**, *24*, 645.
[18] M. Peuster, C. Fink, C. von Schnakenburg, *Biomaterials* **2003**, *24*, 4057.
[19] M. Peuster, C. Hesse, T. Schloo, C. Fink, P. Beerbaum, C. von Schnakenburg, *Biomaterials* **2006**, *27*, 4955.
[20] L. De Rosa, C. R. Tomachuk, J. Springer, D. B. Mitton, S. Saiello, F. Bellucci, *Mater. Corros.* **2004**, *55*, 602.
[21] N. Kumar, R. S. Langer, A. J. Domb, *Adv. Drug Del. Rev.* **2002**, *54*, 889.
[22] D. A. Shipp, C. W. McQuinn, B. G. Rutherglen, R. A. McBath, *Chem. Commun.* **2009**, 6415.
[23] B. G. Rutherglen, R. A. McBath, Y. L. Huang, D. A. Shipp, *Macromolecules* **2010**, *43*, 10297.
[24] Q. Lou, D. A. Shipp, *ACS Appl. Mater. Interfaces* **2012**, *4*, 4457.
[25] F. Sammoura, K. B. Lee, L. W. Lin, *Sens. Actuators, A* **2004**, *111*, 79.
[26] W. F. Ng, K. Y. Chiu, F. T. Cheng, *Mater. Sci. Eng., C* **2010**, *30*, 898.
[27] G. L. Song, *Corros. Sci.* **2007**, *49*, 1696.
[28] Y. Lee, S. Bang, I. Lee, Y. Kim, G. Kim, P. Dutta, D. Sylvester, D. Blaauw, *IEEE J. Solid-State Circuits* **2013**, *48*, 229.